Preprints of the 21st IFAC World Congress (Virtual)
Berlin, Germany, July 12-17, 2020

A Load Power Sharing Strategy for Virtual Oscillator-based Photovoltaics Generation in Islanded Microgrid

Trung Tran Thai*, David Raisz*, Antonello Monti*
Han Min Htut**

** Institute for Automation of Complex Power Systems, E.ON Energy Research Center, RWTH Aachen University (e-mail: {ttrung; amonti; draisz@eonerc.rwth-aachen.de).*
*** Sirindhorn International Thai-German Graduate School of Engineering (TGGS) (e-mail: han.m-epe2017@tggs.kmtnb.ac.th)*

Abstract: This paper proposes a method to control the power-sharing between parallel-connected photovoltaics generation in an islanded microgrid. The two-stage converter-based PV generation is used combined with modified virtual oscillator control and cascade sliding mode control. With this proposed control configuration, the power-sharing in proportion to the inverter power rating and maximum power point tracking is guaranteed autonomously without the need of energy storage systems, while maintaining the primary advantages of the virtual oscillator control method. The effectiveness of the proposed control scheme is validated through simulations in MATLAB/Simulink.

Keywords: Photovoltaics (PV), Virtual Oscillator Control (VOC), Cascade Sliding Mode Control (CSMC) Maximum Power Point Tracking (MPPT), Two-stage Converter.

1. INTRODUCTION

The concept of microgrid has emerged, from the view of the utility's standpoint, in order to utilize the advantages of integrating distributed generation units (DGs) and solve the concerns related to the control of power system components such as DGs, loads and other relating equipment. Generally, the microgrid is a controllable small-scale power system consisting of DGs, energy storage systems (ESSs), and local loads that can be operated in both grid-connected and islanded mode (Hossain et al., 2019). On the other hand, the deployment of renewable energy sources (RESs) such as Photovoltaics (PV) and wind energy, has increased due to environmental and economic concerns. With the advantages such as ease of installation, less maintenance and long lifetime, the PV sources become the most promising renewable energy sources (Farret and Simoes, 2006).

Due to the stochastic nature of the PV resources, the generated power from them is fluctuating. In addition, it is preferable to operate at a maximum power point (MPP) for PV sources to maximize the produced energy (Bacha et al., 2015). On the other hand, it is necessary to regulate the voltage and frequency of the microgrids to ensure the stability, especially when operating in the islanded mode. However, as the PV penetration increases, the maximum power point tracking (MPPT) will affect the stability of the microgrid (Denholm and Margolis, 2007). According to (Matos et al., 2015, Mahmood et al., 2014), to ensure the load/generation power balance and to regulate voltage and frequency in an islanded microgrid with intermittent sources like PV, the energy storage systems (ESS) are crucial. Although ESS could be the simplest solution, this will also increase the costs of the system (Cai et al., 2017).

Different methods have been proposed in the literature to overcome these issues. In (Elrayyah et al., 2014), a hybrid controller with a switch between the so-called fast MPPT controller and the slow MPPT for microgrid-integrated PV sources is presented. The value of *dp/dv* is used as a threshold to control switching between controllers. The universal controller was proposed in (Elrayyah et al., 2015) where the need of dc-link voltage regulation and maximum power point tracking (MPPT) is achieved autonomously without needing reconfiguration of the control system. The improved dual droop control scheme was proposed in (Liu et al., 2017) to control the two-stage converters with PV sources where the dc-link voltage of each converter is allowed to drop a little whenever the PV capacity cannot meet its droop command. By doing this, the droop power command is reduced, which will allow the converter with enough capacity to increase its generation to meet the load demand. In these above papers, the decentralized control method, namely, droop control is used as the main controller for the voltage source inverter (VSI).

On the other hand, the new decentralized control method, namely the virtual oscillator control (VOC), for the single-phase microgrid and the three-phase microgrid was introduced in (Johnson et al., 2014b, Dhople et al., 2013), respectively, to ensure power-sharing and synchronization of parallel inverters in islanded microgrids. In (Johnson et al., 2016), the detailed design strategy for the virtual oscillator is presented with experimental validation. While providing droop like voltage

and frequency regulation control in the steady state, this decentralized control method (VOC) has some advantages over droop control method such as less computational burden since it acts on instantaneous measurements which leads to a faster and better damped response for dynamic performance (Johnson et al., 2017). When PV sources are interfaced through virtual oscillator controlled voltage source inverters with microgrid, the way to add maximum power point tracking (MPPT) control loop to VOC is presented in (Johnson et al., 2014a). However, there is still a need for the energy storage system (ESS) to maintain the voltage of the islanded microgrid.

Inspired by (Liu et al., 2017, Johnson et al., 2014a, Elrayyah et al., 2015), in this paper, the control method for parallel-connected PV based two-stage converters constituting dc-dc boost converters and VOC-based inverter is presented in order to achieve maximum power point tracking whenever necessary while ensuring the load-power sharing and maintaining the voltage and frequency stability of the islanded microgrid with high penetration of the PV sources without the need of energy storage system (ESS).

The rest of this paper is organized as follows. In Section II, the overall proposed control scheme is explained in detail. Section III discusses the effectiveness of the proposed controller with the simulation results of the test system and the paper concludes in Section IV.

2. PROPOSED CONTROLLER DESIGN

In this Section, the configuration of the islanded microgrid considered in this work along with the proposed control scheme is presented.

The test system is shown in Fig. 1 consisting of two parallel-connected DGs to serve a common load at the point of common coupling (PCC). In addition, a distribution line is modeled by a resistance (R_{line}) in series with an inductance (L_{line}) between each DG and PCC. V_{dc}, I_{dc}, i_L, $i_{f(abc)}$ are the dc-link voltage, current, inductor current of the boost converter, and the inductor current from LCL filter, respectively.

The general schematic of the proposed control strategy is also presented in Fig. 1, which consists of a cascaded SMC, and modified VOC. DG-2 has the same control configuration and electric connection as DG-1.

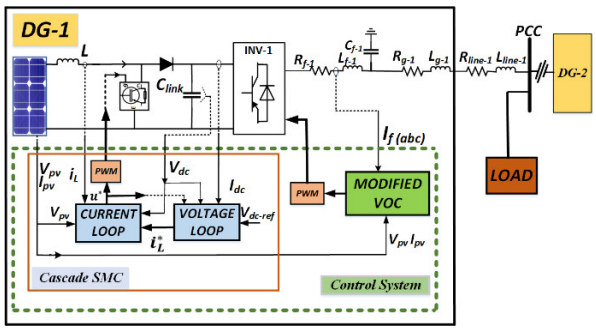

Fig. 1. Schematic control diagram of the test system with proposed control strategy.

According to the control configuration from Fig. 1, the CSMC is used to control dc-link voltage, while the modified VOC is designed to guarantee voltage and frequency regulation, and power-sharing under different load and solar irradiation conditions without the need of ESS. The control objectives of this paper are: 1) to guarantee the load power-sharing according to inverter rated power when the power output of the PV sources satisfy the power-sharing ratio, and 2) to force the PV to operate in MPP mode if the power generation from PV is lower than the requirement for power-sharing. The detailed controller design is explained as follows.

2.1. *Cascaded Sliding Mode Control of DC-DC Boost Converter*

The dc-dc boost converters are usually used in PV systems due to their simplicity and robustness. In boost converter with changing input voltage, the dc output voltage has to be controlled to achieve the desired value. The dc-dc boost converter with an ideal switch (Guldemir, 2005) is shown in Fig. 2.

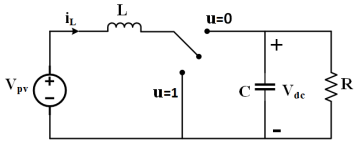

Fig. 2. DC-DC boost converter with an ideal switch.

In this paper, a cascaded sliding mode control (CSMC) is used to control the output voltage of boost converter because of its superior dynamic, accuracy and robustness against internal and external disturbances (Zhang et al., 2015, Asma et al., 2017). In general, SMC is designed to force the system state variables onto the predefined sliding surface and then keep them close to a neighborhood of this surface.

The expected form of the final SMC control law is given as:

$$u^* = u_{re} + u_{sw}$$

where: u_{re} is a *reaching law* that is defined from system state equations, and u_{sw} is a discontinuous *switching law* classically chosen as a signum function *sgn*.

By applying Kirchhoff's voltage and current laws, the dynamics of the boost converter is obtained as follows:

$$\frac{dV_{dc}}{dt} = \frac{-V_{DC}}{RC} + \frac{1}{C}(1-u)i_L \qquad (1)$$

$$\frac{di_L}{dt} = \frac{V_{pv}}{L} - \frac{V_{dc}}{L}(1-u) \qquad (2)$$

where R is the equivalent impedance at the output of the boost converter, u is the duty cycle signal used to control the converter.

The proposed CSMC scheme consists of two control loops (the inner current loop and the outer voltage loop) for regulating

the dc output voltage of the boost converter. For the inner current control loop, the sliding surface is chosen as:

$$S_I = K_{1-I}\left(i_L^* - i_L\right) + K_{2-I}\int\left(i_L^* - i_L\right)dt \tag{3}$$

where K_{1-I} and K_{2-I} are designed coefficients of the sliding surface, i_L^* is the current reference obtained from the output of the outer voltage control loop.

Taking time derivative of (3), then substituting $\frac{di_L}{dt}$ from (2) to (3), we have:

$$\begin{aligned}\frac{dS_I}{dt} &= \frac{1}{L}\left(V_{dc} - V_{pv}\right)K_{1-I} + K_{2-I}\left(i_L^* - i_L\right) \\ &\quad -\frac{1}{L}K_{1-I}V_{dcu} = F_i - D_i u\end{aligned} \tag{4}$$

Here we introduce $F_i = \frac{1}{L}\left(V_{dc} - V_{pv}\right)K_{1-I} + K_{2-I}\left(i_L^* - i_L\right)$ and $D_i = \frac{1}{L}K_{1-I}V_{dc}$ for the sake of simplicity. Solving $\frac{dS_I}{dt} = 0$, the reaching law u_{re} is defined as follows:

$$u_{re} = \frac{F_i}{D_i} \tag{5}$$

The switching term of the control law is chosen as a simple discontinuous *sat* function defined as follows:

$$u_{sw} = -K_{3-I}\,sat\left(S_I\right) \tag{6}$$

where:

$$sat\left(S_I\right) = \begin{cases} sgn(S_I) & \text{if } S_I > \phi \\ S_I/\phi & \text{if } S_I \le \phi \end{cases} \tag{7}$$

According to (7), the value of ϕ parameter is selected with respect to the thickness of the chattering. In this paper, ϕ is chosen as 0.5 to maintain the trade-off between system performance and robustness of the proposed controller against uncertainties.

From (5) and (6), the complete control law of the inner current loop is given by:

$$u^* = \frac{F_i}{D_i} - K_{3-I}\,sat\left(S_I\right) \tag{8}$$

In the following, we use the Lyapunov stability criterion to analyze the stability of the proposed inner current control loop. The Lyapunov function can be chosen as follows:

$$V = \frac{1}{2}S_I^2 \tag{9}$$

Taking the derivative of V with respect to time:

$$\frac{dV}{dt} = S_I\frac{dS_I}{dt} \tag{10}$$

Substituting $\frac{dS_I}{dt}$ from (4) with u^* given in (8) into (10):

$$\begin{aligned}\frac{dV}{dt} &= S_I\left\{F_i - D_i\left(\frac{F_i}{D_i} - K_{3-I}\,sat\left(S_I\right)\right)\right\} \\ &= -K_{3-I}S_I\,sat\left(S_I\right)\end{aligned} \tag{11}$$

From (9) and (11), it can be seen that with $K_{3-I} > 0$ the Lyapunov function and its time derivative is positive definite and negative semi-definite, respectively. Hence, the proposed inner current loop is asymptotically stable.

Similarly, the outer voltage control loop is designed with the expected form of the final SMC control law is given as:

$$i_L^* = i_{L\_re} + i_{L\_sw}$$

Choosing the sliding surface as follows:

$$S_V = K_{1-V}\left(V_{dc}^* - V_{dc}\right) + K_{2-V}\int\left(V_{dc}^* - V_{dc}\right)dt \tag{12}$$

Taking time derivative of (12), then substituting $\frac{dV_{dc}}{dt}$ from (1) to (12), we have:

$$\begin{aligned}\frac{dS_V}{dt} &= \frac{V_{dc}}{RC}K_{1-V} + K_{2-V}\left(V_{dc}^* - V_{dc}\right) + \frac{u-1}{C}i_L \\ &= F_v - D_v i_L\end{aligned} \tag{13}$$

Here we introduce $F_V = \frac{V_{dc}}{RC}K_{1-I} + K_{2-I}\left(V_{dc}^* - V_{dc}\right)$ and $D_V = -\frac{(u-1)}{C}$ for the sake of simplicity. Solving $\frac{dS_V}{dt} = 0$, the reaching law i_{L_re} is defined as follows:

$$i_{L\_re} = \frac{F_V}{D_V} \tag{14}$$

In order to minimize the chattering phenomenon, the switching term of the outer voltage control loop is chosen using the super twisting algorithm (STA) (Liu, 2017) governed by:

$$i_{L\_sw} = -K_{3-V}sgn\left(S_V\right) - K_{4-V}\left|S_V\right|^{K_{5-V}}sgn\left(S_V\right) \tag{15}$$

Hence, the complete control law of the voltage control loop is given as follows:

$$i_L^* = \frac{F_V}{D_V} - K_{3-V}sgn\left(S_V\right) - K_{4-V}\left|S_V\right|^{K_{5-V}}sgn\left(S_V\right) \tag{16}$$

Thanks to the Lyapunov stability criterion, the stability of the proposed voltage control loop is analyzed by choosing the Lyapunov function *W* as:

$$W = \frac{1}{2}S_V^2 \tag{17}$$

Taking the time derivative of W and substitute i_L^* from (16) we have

$$\frac{dW}{dt} = D_V\left(K_{3-V} + K_{4-V}\left|S_V\right|^{K_{5-V}}\right)S_V sgn\left(S_V\right) \tag{18}$$

Since the duty cycle signal is between $0 \le u^* \le 1$, the term $D_V \le 0$. From (17) and (18), it can be seen that the Lyapunov function is positive definite and its time derivative is negative

semi-definite with $K_{3-V} > 0$ and $K_{4-I} > 0$. Therefore, the proposed voltage control loop is asymptotically stable.

2.2. Modified Virtual Oscillator Controller (VOC)

The modified VOC utilized in this paper is shown in Fig. 3. This control logic measures the inverter output filter inductor current $i_{f\alpha}$ and its output v^*_{VOC} is used to generate the PWM modulation signals. The oscillator consists of a negative damping resistor R_{VOC}, a resonant $L_{VOC}C_{VOC}$ circuit that sets the system frequency, and a nonlinear cubic voltage-dependent current source for sustaining the oscillation.

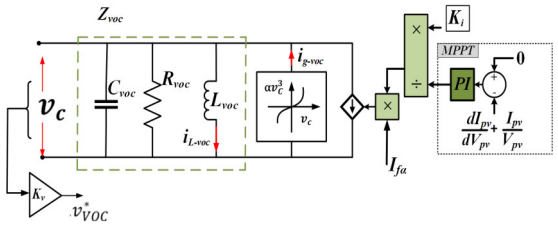

Fig. 3. Schematic diagram of modified VOC.

Applying Kirchhoff's voltage and current laws, the dynamics of the VOC are obtained as follows:

$$L_{voc}\frac{di_{L\_voc}}{dt} = \frac{v_c}{K_v} \tag{19}$$

$$C_{voc}\frac{dv_c}{dt} = -\alpha\frac{v_c^3}{K_v^2} - \sigma v_c - K_v i_{L\_voc} - K_v K_i i_{f\alpha} \tag{20}$$

where: $\sigma = -1/R_{voc}$, and K_v, K_i are voltage and current scaling factors, respectively.

Differentiating (20) and substituting (19), the VOC dynamics can be rearranged as:

$$C_{voc}\frac{d^2v_c}{dt^2} = \varepsilon\omega\sigma\left(1-\beta v_c^2\right)\frac{dv_c}{dt} - \omega^2 v_c - \varepsilon\omega K_i\frac{di_{f\alpha}}{dt} \tag{21}$$

where: $\beta = \frac{3\alpha}{\sigma}$, $\varepsilon = \sqrt{\frac{L_{voc}}{C_{voc}}}$, and $\omega = \frac{1}{\sqrt{L_{voc}C_{voc}}}$

The determination of parameters for VOC is adopted from (Johnson et al., 2016) and the necessary equations and procedure are presented briefly in the following.

- The maximum and minimum voltage variation is defined as *±10%* and the scaling factors are chosen based on $K_v = V_{\max}$ and $K_i = 3V_{\min}/P_{rated}$.
- The conductance, $\sigma = \frac{V_{\max}}{V_{\min}}\frac{V_{\max}^2}{V_{\max}^2 - V_{\min}^2}$ and the coefficient of the cubic current source, $\alpha = 2\sigma/3$ is selected.
- It is needed to satisfy the angular frequency, $\omega_n = \left(\sqrt{L_{voc}C_{voc}}\right)^{-1}$ and the resistance, $R_{voc} \geq \sigma^{-1}$ when choosing R_{voc}, L_{voc} and C_{voc} values in addition to maximum frequency variation $\Delta\omega$, the maximum rise time $t_{rise}^{\max}$ and the maximum ratio of the third to first harmonics $\delta_{\max}$.

If the voltage and frequency become out of predetermined limits with the change in load, the above steps have to be repeated.

As seen from Fig. 3, in order to utilize universal control purposes, the MPPT control algorithm based on the incremental conductance (IC-MPPT) method is used to modify the current scaling factor K_i. The basis of the IC-MPPT algorithm is presented in Fig. 4, in which the PV sources will operate at the MPP if the condition $\frac{dP_{pv}}{dV_{pv}} = 0$ is satisfied (Putri et al., 2015, Chafle and Vaidya, 2013). Manipulating this condition, we have:

$$\frac{dP_{pv}}{dV_{pv}} = \frac{d\left(V_{pv}I_{pv}\right)}{dV_{pv}} = I_{pv} + V_{pv}\frac{dI_{pv}}{dV_{pv}} \tag{22}$$

Since $\frac{dP_{pv}}{dV_{pv}} = 0$ at MPP, then:

$$I_{pv} + V_{pv}\frac{dI_{pv}}{dV_{pv}} = 0 \tag{23}$$

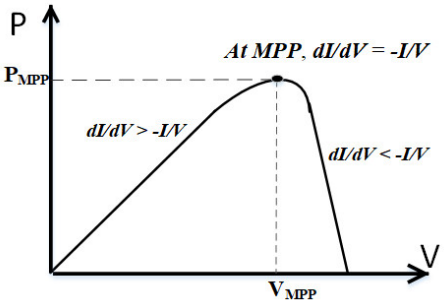

Fig. 4. Schematic diagram of modified VOC.

A PI controller is implemented to satisfy (23), then its output K_{mpp} is used to modify the current scaling factor K_i in order to adjust inverter power output based on different solar irradiation. K_{mpp} is limited between 1 and 100 where $K_{mpp} = 1$ indicates that the PV source operates at the power-sharing mode. Inspired by the natural characteristics of VOC, that the inverter power output is inverse proportional to the current scaling factor, the modified input of the VOC will be $I'_{f\alpha} = \frac{K_i}{K_{MPP}}I_{f\alpha}$.

3. SIMULATION RESULTS AND DISCUSSION

In this section, the effectiveness of the proposed control strategy is validated in MATLAB/Simulink. The schematic diagram of the test system is presented in Fig. 1. The nominal phase to phase voltage and frequency is 400 V and 50 Hz, respectively. The physical parameters of each DG used in this particular case study are given in Table 1.

Table 1. Power System Parameters

Description	Inverter 1, 2
Rated Power	15 kVA
Inverter-side filter inductance	629 μH
Load-side filter inductance	377 μH
Filter capacitance	15 μF
Line impedance (R_{line}, X_{line})	0.003 Ω, 0.003 Ω
DC-link reference voltage	800 V
DC-link capacitance	600 μF

The control system parameters are summarized as follows, in which the gains of CSMC and PI controller have been tuned based on trial and error method:

- VOC Controller: Oscillator Parameters: R_{voc}=0.2705 Ω, L_{voc}=52.087 μH, C_{voc}=194.5 mF, voltage and current scaling factors: K_v=254.0341, K_i=0.0416.
- SMC Controller: $K_{1-I} = 0.083$, $K_{2-I} = 1.43$, $K_{1-V} = 0.56$, $K_{2-V} = 7.6$, $K_{3-I} = 130$, $K_{3-V} = 0.188$, $K_{4-V} = 1$, and $K_{5-V} = 0.5$.
- PI Controller: $K_p = 10$, K_I =150.

Two different case studies are simulated to analyze the effectiveness of the proposed scheme as described in the following sub-sections. The case studies validate the controller performance subject to load power-sharing in a normal irradiation condition, i.e., the power outputs of two DGs are able to supply the load power-sharing demand, and critical irradiation condition, i.e., one DG cannot supply the load power-sharing demand, respectively.

3.1. Two DGs with high solar irradiation sharing a common load

In this first scenario, the objective is to validate the power-sharing capability when the power generated from PVs are enough to share the load power in proportion to the inverter rated powers. A 15kW constant power load (CPL) is connected at the PCC. As can be seen from Fig. 5, at the first $t = 0.5$ *s*, both two PV sources operate at 1 pu (1000W/m^2) and share the load power equally (each with 7.55 kW). The dc-link voltages are maintained at 800 V by the SMC and the inverter output voltages are also within the predefined limits. At $t = 0.8$ *s*, the solar irradiation of PV-2 is reduced to 0.7 pu (correspondingly, the maximum available generated power of PV-2 is also reduced). However, the simulation results in Fig. 5 show that the power-sharing ratio of the two DGs remains unchanged. These results confirm that the two DGs share the load demand according to the predefined ratio as long as the power generated from PVs meets the requirement.

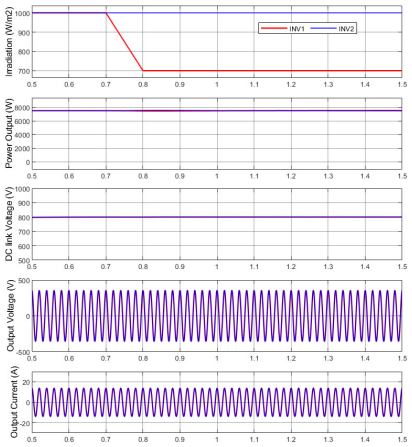

Fig. 5. Simulation results for Case 1.

3.2. One DGs with high solar irradiation and another DG with low solar irradiation while sharing a common load

The objective of this case study is to validate the performance of the MPPT mode when the power generated from one DG cannot satisfy the load-sharing requirement. A 15kW CPL is connected at the PCC. At the first t = 0.5 s, both PVs are operated at 1 pu irradiation. Then at $t = 0.7$ *s*, the solar irradiation coming to PV array of DG-2 is reduced to 0.1 pu while that for DG-1 remains unchanged.

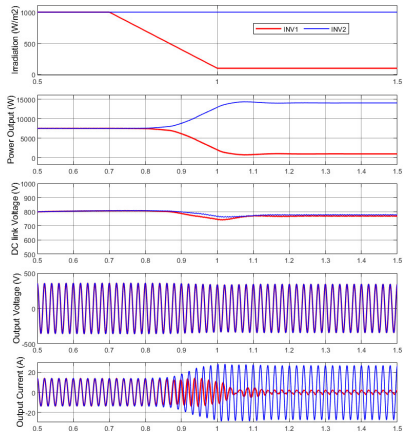

Fig. 6. Simulation results for Case 2.

As can be seen from Fig. 6, when the power output of DG-2 is reduced (from 7.55 kW to 0.92 kW) below the load-sharing requirement, the PI controller starts acting to regulate the current scaling factor to force the PV-2 to operate in MPPT mode. Consequently, to meet the load demand, DG-1 needs to generate more power (from 7.55 kW to 14.19 kW) to compensate for the shortfall. These simulation results confirm that the proposed control strategy can autonomously switch between two operating modes without the need of controller reconfiguration.

4. CONCLUSION

In this paper, a control strategy for controlling the two-stage converter based PV generation in an islanded microgrid is presented. A cascaded sliding mode control is applied to

regulate the dc-link output voltage of boost converters. Meanwhile, an incremental conductance-based MPPT method to track maximum power is combined with the VOC to allow the DGs to operate at different control modes without the need of ESS. The simulation results are carried out in Matlab/Simulink. The simulation results show that:

- The proposed control strategy maintains the load power-sharing in proportion to the inverter rated power, as long as the powers generated from PV arrays satisfy load-sharing requirement.
- The modified VOC effectively forces the PV array to operate at the MPP when the solar irradiation decreases.

The simulation results show that the proposed control strategy allows the PV systems to operate at different operating modes without the need of controller reconfiguration. However, there is a slight error in tracking the MPP. Therefore, an important direction for future research is to improve the MPPT algorithm to eliminate this tracking error. In addition, a low-irradiation limitation in the operation of the PV system needs to be considered when designing SMC to use the proposed control strategy in practical implementation.

ACKNOWLEDGMENT

The authors gratefully acknowledge funding by the German Federal Ministry of Education and Research (BMBF) within the Kopernikus Project ENSURE 'New Energy grid StructURes for the German Energiewende'

REFERENCES

Asma, C., Abdelaziz, Z. & Nadia, Z. 2017. Dual loop control of DC-DC boost converter based cascade sliding mode control. *2017 International Conference on Green Energy Conversion Systems (GECS).*

Bacha, S., Picault, D., Burger, B., Etxeberria-Otadui, I. & Martins, J. 2015. Photovoltaics in Microgrids: An Overview of Grid Integration and Energy Management Aspects. *IEEE Industrial Electronics Magazine.*

Cai, H., Xiang, J., Chen, M. Z. Q. & Wei, W. 2017. A decentralized control strategy for photovoltaic sources to unify MPPT and DC-bus voltage regulation. *2017 American Control Conference (ACC).*

Chafle, S. R. & Vaidya, U. B. 2013. Incremental conductance MPPT technique FOR PV system. *International Journal of Advanced Research in Electrical, Electronics and Instrumentation Engineering,* 2**,** 2720-2726.

Denholm, P. & Margolis, R. M. 2007. Evaluating the limits of solar photovoltaics (PV) in electric power systems utilizing energy storage and other enabling technologies. *Energy Policy,* 35**,** 4424-4433.

Dhople, S. V., Johnson, B. B. & Hamadeh, A. O. 2013. Virtual Oscillator Control for voltage source inverters. *2013 51st Annual Allerton Conference on Communication, Control, and Computing (Allerton).*

Elrayyah, A., Sozer, Y. & Elbuluk, M. 2015. Microgrid-Connected PV-Based Sources: A Novel Autonomous Control Method for Maintaining Maximum Power. *IEEE Industry Applications Magazine.*

Elrayyah, A., Sozer, Y. & Elbuluk, M. E. 2014. Modeling and Control Design of Microgrid-Connected PV-Based Sources. *IEEE Journal of Emerging and Selected Topics in Power Electronics,* 2**,** 907-919.

Farret, F. A. & Simoes, M. G. 2006. *Integration of alternative sources of energy*, John Wiley & Sons.

Guldemir, H. 2005. Sliding mode control of DC-DC boost converter. *Journal of Applied Sciences,* 5**,** 588-592.

Hossain, M. A., Pota, H. R., Hossain, M. J. & Blaabjerg, F. 2019. Evolution of microgrids with converter-interfaced generations: Challenges and opportunities. *International Journal of Electrical Power & Energy Systems,* 109**,** 160-186.

Johnson, B., Rodriguez, M., Sinha, M. & Dhople, S. 2017. Comparison of virtual oscillator and droop control. *2017 IEEE 18th Workshop on Control and Modeling for Power Electronics (COMPEL).*

Johnson, B. B., Dhople, S. V., Cale, J. L., Hamadeh, A. O. & Krein, P. T. 2014a. Oscillator-Based Inverter Control for Islanded Three-Phase Microgrids. *IEEE Journal of Photovoltaics,* 4**,** 387-395.

Johnson, B. B., Dhople, S. V., Hamadeh, A. O. & Krein, P. T. 2014b. Synchronization of Parallel Single-Phase Inverters With Virtual Oscillator Control. *IEEE Transactions on Power Electronics,* 29**,** 6124-6138.

Johnson, B. B., Sinha, M., Ainsworth, N. G., Dörfler, F. & Dhople, S. V. 2016. Synthesizing Virtual Oscillators to Control Islanded Inverters. *IEEE Transactions on Power Electronics,* 31**,** 6002-6015.

Liu, H., Yang, Y., Wang, X., Loh, P. C., Blaabjerg, F., Wang, W. & Xu, D. 2017. An Enhanced Dual Droop Control Scheme for Resilient Active Power Sharing Among Paralleled Two-Stage Converters. *IEEE Transactions on Power Electronics,* 32**,** 6091-6104.

Liu, J. 2017. Chapter 1 - Basic sliding mode control principle and design. *In:* LIU, J. (ed.) *Sliding Mode Control Using MATLAB.* Academic Press.

Mahmood, H., Michaelson, D. & Jiang, J. 2014. A Power Management Strategy for PV/Battery Hybrid Systems in Islanded Microgrids. *IEEE Journal of Emerging and Selected Topics in Power Electronics,* 2**,** 870-882.

Matos, J. G. D., Silva, F. S. F. E. & Ribeiro, L. a. D. S. 2015. Power Control in AC Isolated Microgrids With Renewable Energy Sources and Energy Storage Systems. *IEEE Transactions on Industrial Electronics,* 62**,** 3490-3498.

Putri, R. I., Wibowo, S. & Rifa'i, M. 2015. Maximum power point tracking for photovoltaic using incremental conductance method. *Energy Procedia,* 68**,** 22-30.

Zhang, J., Dorrell, D. G., Li, L. & Argha, A. 2015. A novel sliding mode controller for DC-DC boost converters under input/load variations. *IECON 2015 - 41st Annual Conference of the IEEE Industrial Electronics Society.*